Recent Advances in Composites Forming Simulation with User-Defined Material Models in Abaqus

James A. Sherwood, Lisa M. Dangora, Kari D. White and Matteo J. Polcari

University of Massachusetts Lowell
Department of Mechanical Engineering
1 University Ave., Lowell, MA 01854

***Abstract**: Thermoforming and automated fabric placement processes show promise for reducing the time and cost for the manufacture of textile-reinforced composites. Simulating these processes can give insight into the manufacturability of the composite structure for each option and guide the design of the manufacturing process. Commonly used fishnet algorithms offer a computationally efficient method for modeling the draping of a fabric on a surface but do not consider the mechanical behavior of the material. A finite element solution for draping has the advantage of including the mechanical behavior of the textile, thereby allowing for investigating the relationship among changes in processing conditions and the resulting quality of the part. In the current research, a finite element based methodology for simulating the behavior of textile reinforced composites during the manufacturing process is presented. The paper will start with an overview of the relatively simple tension, compression, bending and shear characterization tests that are used to provide inputs to the model for capturing the mechanical behavior of the textile. The ability of the model will be demonstrated (1) for the forming of a military helmet from a thermoplastic fiber-reinforced thermoplastic matrix to predict the precipitation of defects and their respective size and (2) for the simulation of automatic fabric placement in wind blade manufacturing for eliminating the forming of out-of-plane waves.*

***Keywords**: Bending, Composites, Fabrics, Forming, Manufacturing, Mechanical Behavior.*

1. Introduction

Currently, the manufacture of composite parts and structures is dominated by manual labor processes. Such processes are time consuming and can result in part-to-part variability. For composite materials to increase market penetration, low-cost high-volume manufacturing processes must become as widespread for composites as they are for the stamping of steel and aluminum sheets. Thermoforming and automated fabric placement processes show promise to meet this objective for the manufacture of textile-reinforced composites. However, the draping of textiles and fabric sheets on compound-curvature surfaces can present challenges. For example, forming processes can lead to wrinkling of the composite reinforcement which can result in premature failure (Hallett, Jones and Wisnom, 2013). Thus, it is important that the manufacturing process be designed to mitigate formation of such unwanted shape distortions. As a result, the processing parameters will be driven by the forming limits of the material and the relative complexity of the part geometry. Unfortunately, the processing conditions that create an environment which is conducive for wrinkle development are not always known before the development phase. A simulation tool that can perform the design-build-test activity in a virtual setting would provide a cost-effective and time-efficient solution to product development and process design.

Commonly used fishnet algorithms offer a computationally efficient method for modeling the draping of a fabric on a surface but do not consider the mechanical behavior of the material. A finite element solution for draping has the advantage of including the mechanical behavior of the textile, thereby allowing for investigating the relationship among changes in processing conditions and the resulting quality of the part. Simulating these processes can give insight into the manufacturability of the composite structure for each option and guide the design of the manufacturing process.

This paper presents two examples of the application of a discrete mesoscopic finite element model. This modeling approach has the potential to provide information regarding thickness changes, fiber orientations, stresses and strains throughout the forming process. The models can identify if and where macroscopic defects such as in-plane waviness, out-of-plane buckling and fabric tearing shown in Figure 1 may occur. The model can then be used to investigate how changes in the processing conditions can mitigate these compromises on part quality.

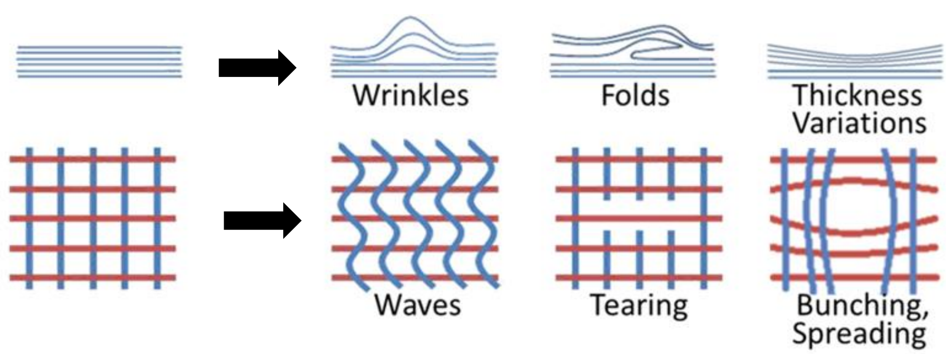

Figure 1. Through-thickness and in-plane forming defects associated with textile composites.

2. Fabric Modeling Approach

The fabric modeling method used in this research is a beam-shell model. Figure 2 shows a schematic of fabric architecture and associated representative unit cell for a woven and a non-crimp fabric reinforcement. The beam elements on the edges of the unit cell capture the mechanical behaviors of the tows; the shell element represents the shear properties of the fabric. The details of this model are given by Jauffrès, Sherwood, Morris, and Chen (2010).

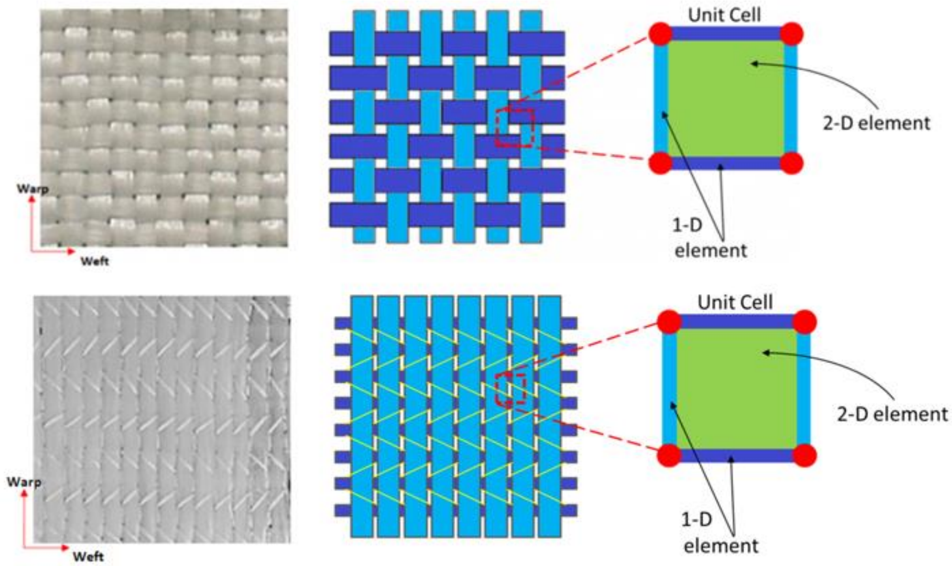

Figure 2. Schematic of fabric architecture and associated representative unit cell for (top) woven and (bottom) non-crimp fabric reinforcement.

3. Hemispherical Forming of a Cross-ply Thermoplastic Lamina

This example of a forming simulation in Abaqus is a preliminary study that will lead to simulating the forming of low-velocity military helmets. The hemisphere is a relatively simplified geometry of the helmet. The specific material considered in this project is Dyneema® HB80, a thermoplastic cross-ply containing four unidirectional layers oriented in a $(0/90)_2$ initial fiber configuration. Ultrahigh molecular weight polyethylene (UHMWPE) fibers and a thermoplastic polyurethane (TPU) based matrix comprise the highly fibrous lamina. The complementary characterization of the tensile and flexural properties is first presented. The material characterization methodologies that are described in this paper are not limited to Dyneema® HB80. They are applicable to a wide range of fiber-reinforced material systems. The shear behavior was previously characterized by Dangora, Hansen, Mitchell, Sherwood and Parker (2015). An example of the good correlation between the model and an actual forming experiment is then shown.

3.1 Tensile Testing

3.1.1 Tensile Testing Methodology

The standard test method for breaking force and elongation of textile fabrics (ASTM-D5035) was used to measure the apparent elastic modulus of Dyneema® HB80 as a function of temperature. These tensile experiments were completed on an Instron 4464 universal testing machine. The specimens were tested to failure at the forming temperatures of interest. Use of an extensometer was avoided to prevent damage of the polymer fibers during testing; therefore, the strain measurements were evaluated based on displacement of the clamps. The "apparent" modulus was reported in accordance with the ASTM-D5035 documentation (ASTM, 2010), (Defoirdt, Biswas, De Vriese, Van Acker, Ahsan, Gorbatikh, et al., 2010) (Joffe, Andersons and Wallström, 2003). Statistically insignificant variance in modulus was observed between samples tested under the same conditions for the 0° and 90° degree orientations. Therefore, the experimental schedule was only conducted in the 0° direction. The tested material had an extremely low coefficient of friction (Sekine, Takao, Shoji, Toyama, Kashiwazaki, Sugasawa, et al., 2001), making it difficult to secure the specimens (Heisserer, 2011). Therefore, to improve gripping of the sample and to minimize slippage, 6.35-mm diameter steel pins were used outside the jaws.

To observe the effects of slippage, the influence of gauge length on tensile response was investigated. This study was conducted at room temperature for samples having gauge lengths ranging from 10 to 40 cm in 5-cm increments. It was expected that the influence of slippage would be less prominent for larger gauge lengths. This hypothesis was confirmed by the data shown in Figure 3. As the sample length increased, the curves converged to a single solution. The slopes of stress-strain curves for the longest gauge lengths converged to the expected modulus, which was approximated using the Rule of Mixtures to be between 44 GPa and 48 GPa. The vertical lines on Figure 3 depict the range of strain used in completing the linear regression for slope calculation. As the experimental values converged to 44 GPa, the effect of slippage was assumed to be negligible for specimen lengths greater than or equal to 35 cm. A summary of the apparent moduli for these gauge lengths is provided in Figure 3.

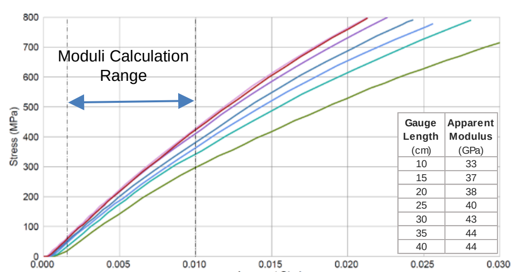

Figure 3. Tensile results for various gauge lengths tested under ambient conditions. Note that the vertical dashed lines indicate the range over which the moduli were calculated.

3.1.2 Tensile Testing Results

Tensile tests were performed on strips of Dyneema® HB80 for temperatures ranging from 70°C to 120°C. For reference, additional data were collected below the possible forming limits at ambient conditions and at 50°C. Load-displacement data collected from the experiments were used to calculate the lamina's apparent modulus as a function of temperature (Figure 4a). As was expected, material compliance increased with increasing temperature. A representative data set was plotted for each of the test conditions (Figure 4b). To avoid damage to the 2-kN load cell, the ambient and 50°C samples were not tested to failure. The data trends indicated that, with an increase in temperature, there were an associated (1) decrease in modulus, (2) reduction in yield strength/strain, and (3) increase in ductility.

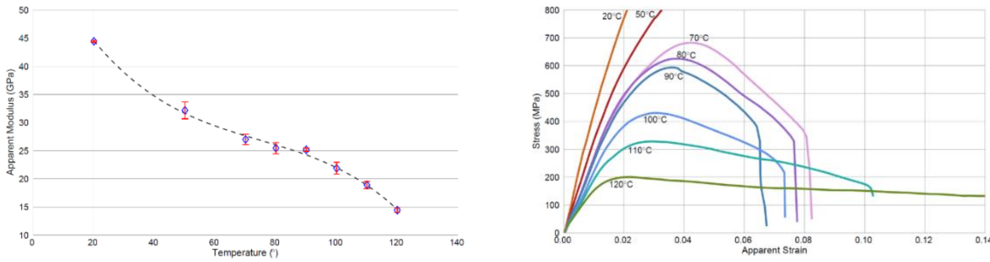

Figure 4. (a) The apparent tensile modulus of Dyneema® HB80 plotted as a function of temperature. (b) Representative tensile data for Dyneema® HB80 tested at various temperatures. Note that the samples at 20°C and 50°C were not tested to failure due to limitations of the load cell.

3.2 Bend Testing

3.2.1 Bend Testing Methodology

The bending rigidity governs the shapes of wrinkles that form during textile draping and composite forming. Thus, it is important to include this property accurately in the finite element model. Unlike conventional isotropic materials, the bending stiffness of fibrous materials is not directly related to the tensile modulus. Therefore, it must be determined through experimentation (Syerko, Comas-Cardona and Binetruy, 2012). The simple vertical cantilever test proposed by Dangora, Mitchell and Sherwood (2015) was modified to accommodate characterization at elevated temperatures.

Figure 5 shows the test fixture used for the bend testing. The sample was heated by radiation from a concentrated ceramic infrared (IR) element. To enforce the cantilever clamped boundary condition at the base of the beam, a magnetic clamp with a pull force of 60-N was used. The free end of the sample was displaced using a hanging mass on a string, redirected with a pulley. The test protocol followed the procedures outlined by Dangora, Mitchell and Sherwood (2015).

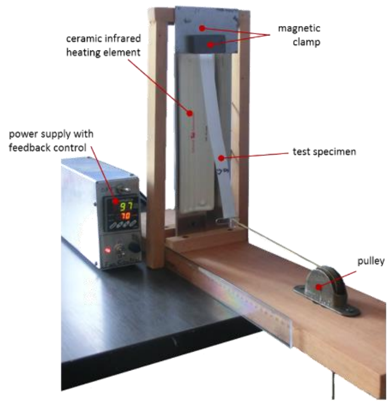

Figure 5. Vertical cantilever method setup for experimental evaluation of bending stiffness at elevated temperatures.

3.2.2 Bend Testing Results

Because there was not enough resolution to differentiate data over a ±10°C temperature variation, bend tests were performed at 80°C, 100°C, and 120°C. The magnitude of the deflection increased with increasing temperature under identical loading conditions. Pictures were taken of the loaded samples, and ImageJ was used to measure discrete displacements. A third-order polynomial was fit to the data, and the curves shown in Figure 6a are the respective fits for an average of three test samples. The curvature was approximated by taking the second derivative of the average deflection equation. Because the force used to displace the cantilever's free end was measured, the moment along the sample was known. This information was used to plot the moment as a function of curvature (Figure 6b). The bending stiffness was derived from the slope of the moment-curvature line, and these values are summarized in Figure 6b. The flexural rigidity did not significantly change over the temperature range investigated, as all values remained on the same order of magnitude.

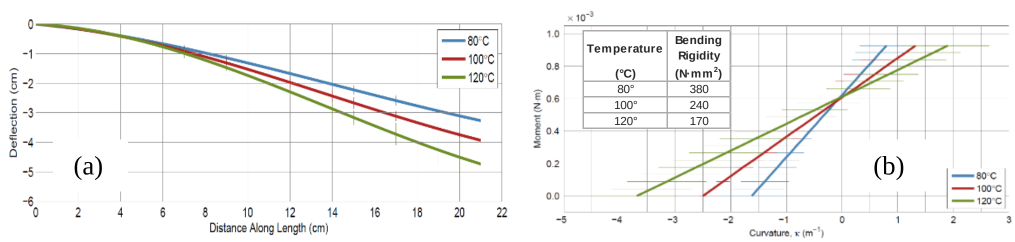

Figure 6. Beam bending. (a) Deflection of strips subject to the same loading at different temperatures and (b) the moment-curvature relation bending at elevated temperature for Dyneema® HB80.

3.3 Comparison of Forming Experiment and Simulation

Hemisphere forming was performed using the experimental setup shown in Figure 7a. The fixture (consisting of a hemispherical punch, an open die, and a blank holder) was placed in an environmental chamber and mounted on a universal testing machine. A single sheet of Dyneema® HB80 was heated to a forming temperature of 100°C and drawn to the punch geometry. Approximately 3200 Pa of pressure was applied to the blank to supply in-plane tension as the sheet was drawn.

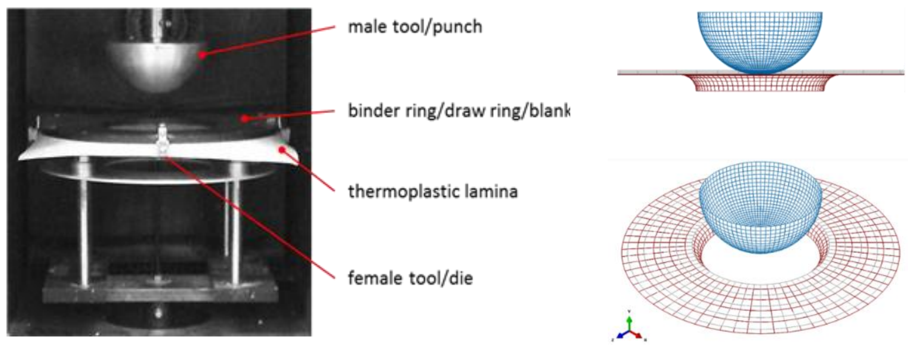

(a) (b)

Figure 7. Hemisphere deep-draw (a) Experimental setup and (b) Associated configuration for FEA.

Similarly, a deep-draw forming simulation was completed in Abaqus/Explicit using the configuration shown in Figure 7b. The tensile modulus and bending stiffness previously measured were used to calculate an effective compressive modulus (E_c) for implementation in the finite element model. The compressive modulus at 100°C was calculated to be 215 MPa and the bilinear modulus was implemented into the finite element model. Note that the lamina properties were assigned to the beam elements, not the fiber properties. A summary of the material constants used in the model are provided in Table 1.

Table 1: Summary of Material Constants for Model Input

Property	Value (MPa)
Tensile Modulus	22,000
Compressive Modulus	215
Shear Stiffness*	$23\|\gamma\|^4 - 55\|\gamma\|^3 + 48\|\gamma\|^2 - 17\|\gamma\| + 3$

*Note that γ is defined as the shear strain of the composite lamina

The experimental and finite element forming results are shown in Figure 8a and Figure 8b, respectively. The laboratory-formed part developed wrinkling at the front, back, and sides of the hemisphere (i.e., along the central axes of the planar sheet but near the bottom of the 3-D part). The finite element analysis was also able to capture the development of such out-of-plane defects in these locations. Overall, the initial modeling efforts show promise and good correlation with wrinkle developed in the physical part during the forming trial.

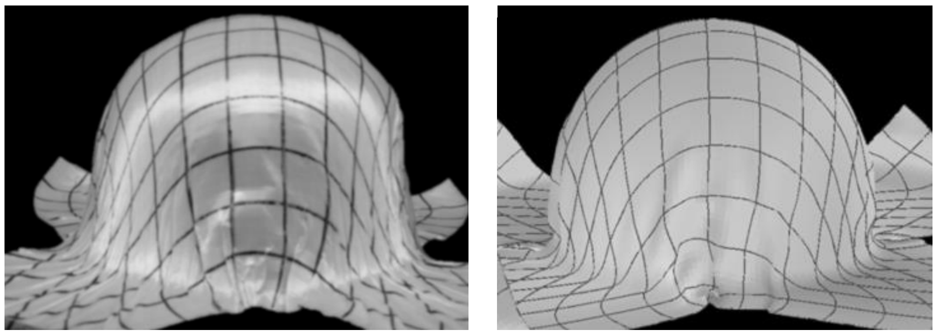

(a) (b)

Figure 8. Dyneema® HB80 sheet formed at 100°C (a) experimentally and (b) virtually via FEA.

4. Automation of Wind Blade Manufacturing using Automated Fabric Placement

Hand layup methods, as shown in Figure 9, are commonly employed for the placement of fabric in the manufacture of composite wind turbine blades. Depending on the mechanical behavior of the fabric and the variabilities associated with manual processes, hand layup methods can result in the random development of localized defects in the preform (Potter, 2009) (Lightfoot, Wisnom and Potter, 2013). These misaligned fibers compromise the load path through the finished part, and out-of-plane wrinkles result in resin-rich zones that compromise part performance and lead to delamination (Bloom, Wang and Potter, 2013). Figure 10 shows an example of a resin-rich pocket associated with an out-of-plane wave, and Figure 11 shows examples of typical failures resulting from such resin-rich areas.

Figure 9. Hand layup of fabric plies in the mold of a wind turbine blade.

The wind blade industry is very interested in introducing automated fabric placement processes for laying material in the mold. Automation can increase the rate of laying material in the mold, thereby increasing the throughput of each set of molds which can cost on the order of $2M. Automation would have the added benefit of having a repeatable system for fabric positioning in the mold, thereby reducing the part-to-part variability. Complementing the automation with a robust model has the potential to reduce the process design time and the shop, labor and material costs associated with prototyping.

This section of the paper presents the status of modeling an automation process that has been developed at Iowa State University (Zhu, 2013). The process uses a pair of rigid grips to do a stepwise shifting of fabric to allow the fabric to conform to the surface of the tool. This modeling uses the beam-shell model to capture the mechanical behavior of the fabric and multiple contacts to consider the interaction of the fabric with the surface of the mold and fabric-placement mechanism.

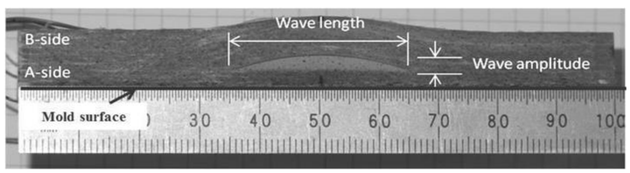

Figure 10. Example of void due to out-of-plane wave in fabric.

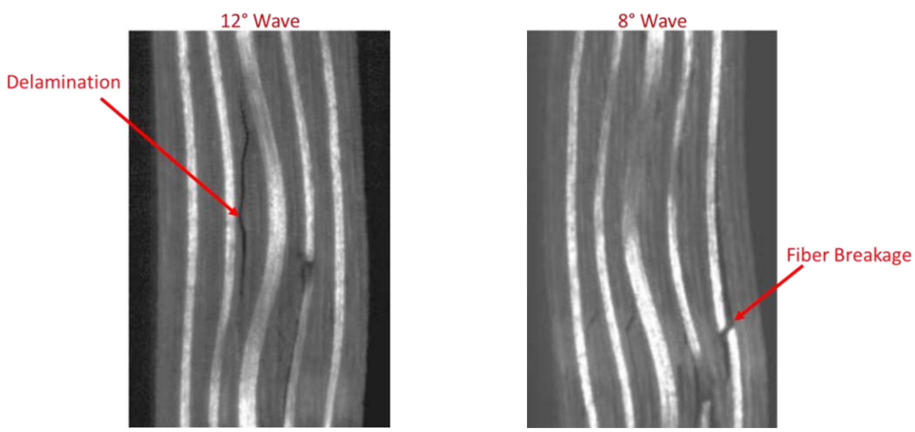

Figure 11. Examples of failure mechanisms due to waves in fibers.

4.1 Shifting Fabric Placement Method

The shifting method uses shearing motions to position discrete sections of a fabric length as shown in Figure 12a. The piecewise continuous shifts on discrete sections allow the fabric conform to a curved path in the mold. Figure 12b shows the result of trying to steer the fabric along an arc without shifting. As a result, the fabric puckers out-of-plane. Figure 12c shows that puckering can be avoided using the piecewise shifting technique.

Figure 13 shows the shifting machine, and Figure 14 shows a close-up of the shifting mechanism and a finite element model of this mechanism. The shifter marches down the length of the blade and lays fabric along a path with a programmed set of shifting movements. Each fabric section has a specified length and magnitude of shift to best approximate the curvature of the mold.

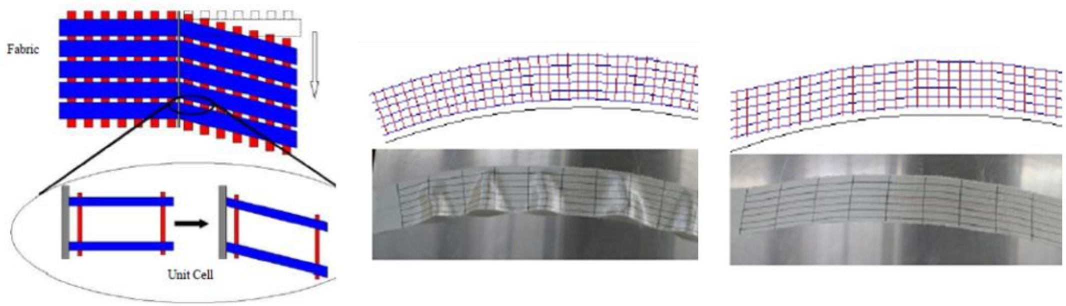

Figure 12. Shifting method: a. Schematic of and comparison of b. steering and c. shifting methods of fabric placement on a curve.

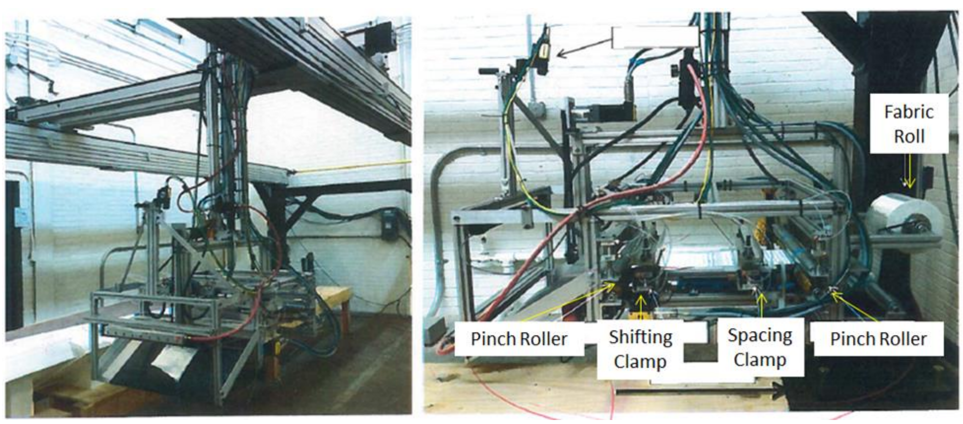

Figure 13. Shifting Machine.

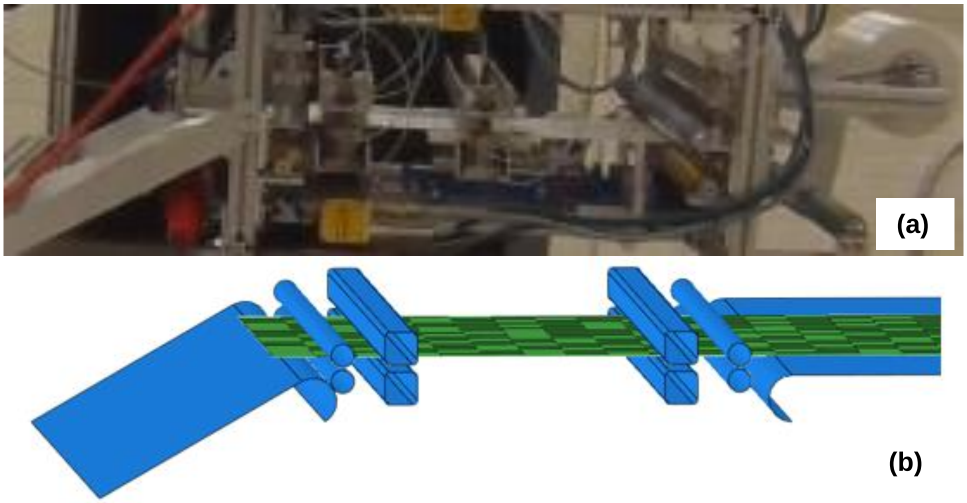

Figure 14. Close-up view of the shifting mechanism (a) physical prototype and (b) finite element model.

4.2 Modeling Results

A fabric blank was represented by a mesh comprised of beam-shell unit cells and placed on a subsection of the mold as a preliminary evaluation of the modeling technique. This evaluation was accomplished by applying displacement boundary conditions directly to the nodes of the fabric mesh to simulate shifting across the length of an entire fabric blank, constrained in space. The next objective was to simulate fabric placement by laying the fabric on a mold surface using similar boundary conditions applied directly to the fabric mesh. This placement was performed on a wind turbine blade trailing edge mold surface, and the results are shown in Figure 15 at four stages of completion.

The next modeling objective was to introduce tooling to perform the fabric placement operations as they are performed by the shifting machine. This placement was attempted initially by using hollow, rigid body grips of 8-mm square cross-section to clamp and move the fabric through the shifting motions. Through trial-and-error of the various contact options that are available in the Abaqus solver, it was realized that the general contact formulation which had been successfully used in the past for forming simulations where the tooling covered a much larger area of the fabric was not well suited to the contact associated with the shifting process. It was discovered that a surface-to-surface contact interaction performed well for the shifting simulation, with the outer thicknesses of the shell elements in the fabric being used as the fabric contact surface. Figure 16 shows the results of a model using round cross-section rigid-body grips to shift the fabric in space.

The final goal in the modeling was to introduce a tray and gravity-feed the fabric smoothly and incrementally down on the mold surface as the fabric was shifted and fed through the machine.

This configuration was accomplished for a flat mold surface and a simplified, generic mold surface and the results of these models are shown in Figures 17 and 18, respectively.

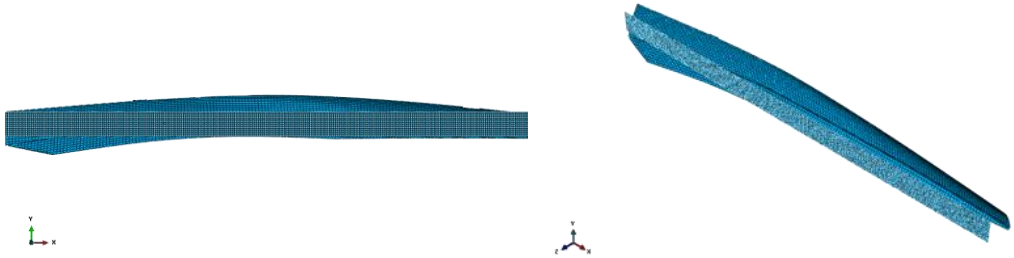

a.

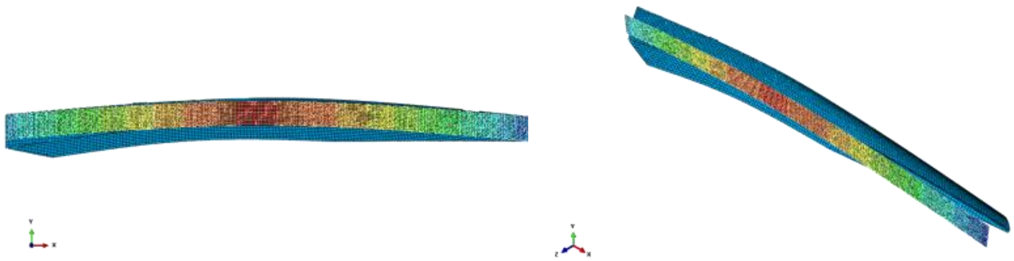

b.

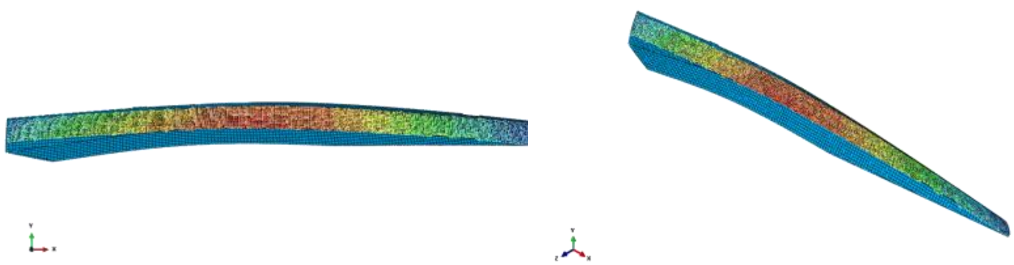

c.

Figure 15. Shifting and layup of fabric blank on mold surface (a.) before shift, (b.) fully shifted and (c.) pressed onto mold, in both x-y and isometric views. Note: The color gradient is the magnitude of displacement in the y direction.

.

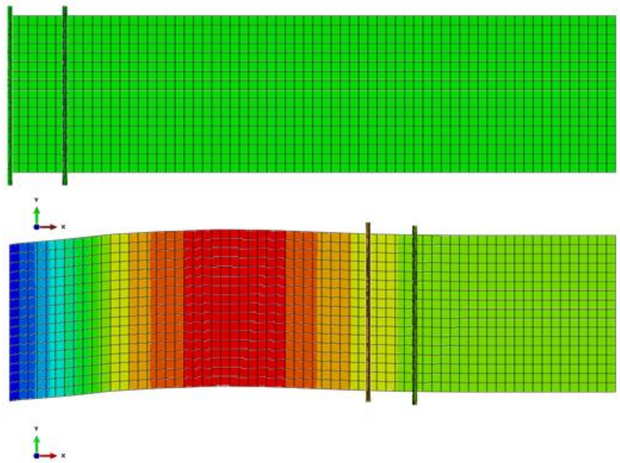

Figure 16. First and last frames of model using rigid body tooling to shift a beam/shell fabric blank into a curved shape in space. Color gradient is displacement in the y-axis direction.

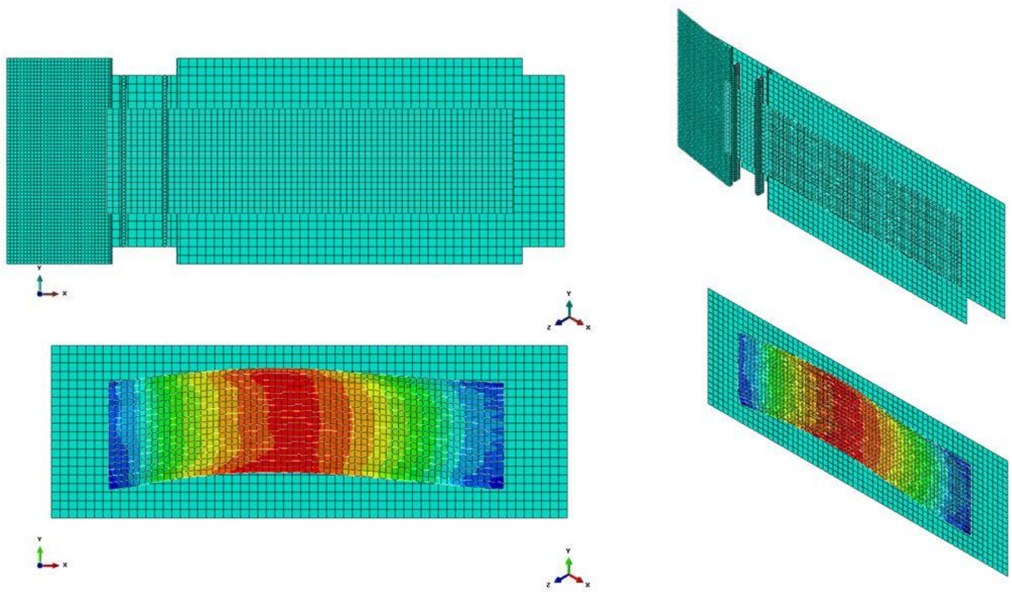

Figure 17. First and last frames of model using rigid body tooling and trays to shift a beam-shell fabric blank into a curved shape and lay it onto a flat mold surface. Color gradient is displacement in the y-axis direction.

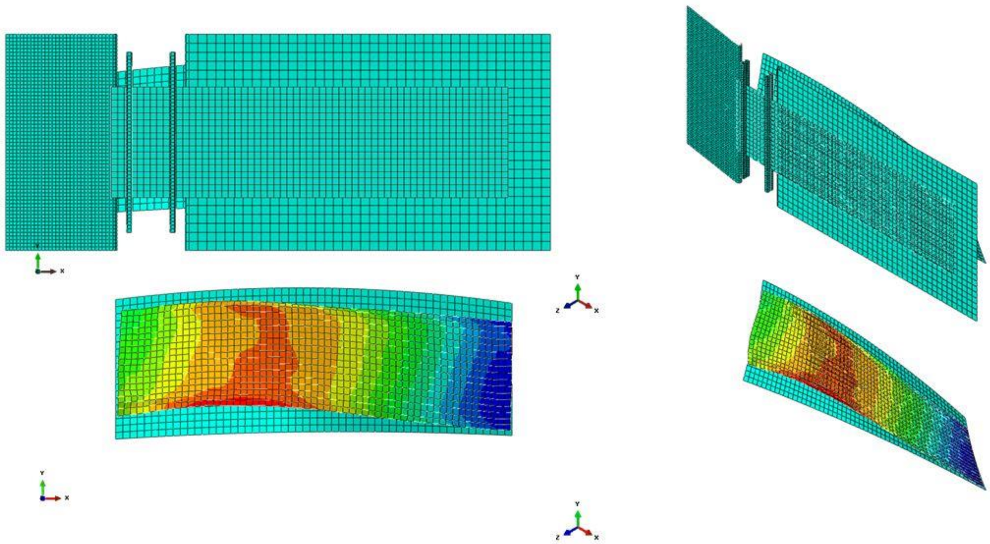

Figure 18. First and last frames of model using rigid body tooling and trays to shift a beam-shell fabric blank into a curved shape and lay it onto a generic double-curvature mold surface. Color gradient is displacement in the y-axis direction.

5. Acknowledgements

The authors thank the US Army Natick Soldier Research, Development and Engineering Center (NSRDEC) for funding this research under contract number W911QY-1A-2-0001 for the support of the helmet forming project. Specifically, the collaboration with Jason Parker is appreciated.

This wind blade material is based upon work supported by the National Science Foundation under Grant Number IIP-1362022 (Collaborative Research: I/UCRC for Wind Energy, Science, Technology, and Research). Any opinions, findings, and conclusions or recommendations expressed in this material are those of the authors and do not necessarily reflect the views of the National Science Foundation. The guidance of Steve Nolet of TPI Composites and Steve Johnson of GE Renewable Energy who are members of the WindSTAR Industrial Advisory Board is greatly appreciated. The model of the shifting mechanism builds upon the machine design work started at Iowa State University by Dr. Matt Frank.

The authors thank the WindSTAR (I/UCRC for Wind Energy, Science, Technology, and Research) IAB for funding of this project.

6. References

1. ASTM International, Standard Test Method for Breaking Force and Elongation of Textile Fabrics (Strip Method). www.astm.org, 2010.
2. Bloom, L. D., J. Wang, and K. D, Potter, “Damage progression and defect sensitivity: An experimental study of representative wrinkles in tension,” Composites Part B: Engineering, 45(1), pp. 449-458, 2013.
3. Dangora L. M., C. J. Hansen, C. J. Mitchell, and J. A. Sherwood, J. C. Parker, “Challenges Associated with Shear Characterization of a Cross-ply Thermoplastic Lamina using Picture Frame Tests,” submitted to Composites Part A: Applied Science and Manufacturing, Volume 78, November 2015, pp. 181-190, 2015.
4. Dangora L. M., C. J. Mitchell, and J. A. Sherwood, “Predictive Model for the Detection of Out-of-Plane Defects Formed during Textile-Composite Manufacture,” Composites Part A: Applied Science and Manufacturing, Volume 78, November 2015, pp. 102-112, 2015.
5. Defoirdt N., S. Biswas, De L. Vriese, J. Van Acker, Q. Ahsan, L. Gorbatikh, et al., “Assessment of the tensile properties of coir, bamboo and jute fibre,” Composites Part A: applied science and manufacturing, Volume 41, Issue 5, May 2010, pp. 588-595, 2010.
6. Hallett SR, Jones MI, Wisnom MR. Tension and compression testing of multi-sirectional laminates with artificial out of plane wrinkling defects. CompTest 2013-Book of Abstracts, Volume59, 2013.
7. Heisserer U. Tensile properties of Dyneema® HB plies (HB2, HB26, HB50, HB80). Technical report. DSM-Dyneema. 2011.
8. Jauffrès D., J. A. Sherwood, C. D. Morris and J. Chen, “Discrete mesoscopic modeling for the simulation of woven-fabric reinforcement forming,” International Journal of Material Forming, Volume 2, Issue 2, pp. 1205-16. 2010
9. Joffe R, J. Andersons and L. Wallström, “Strength and adhesion characteristics of elementary flax fibres with different surface treatments,” Composites Part A: Applied Science and Manufacturing, Volume 34, Issue 7, pp. 603-12, 2003.
10. Lightfoot, J. S., M. R. Wisnom and K. Potter, "Defects in woven preforms: Formation mechanisms and the effects of laminate design and layup protocol," Composites Part A: Applied Science and Manufacturing, Volume 51, pp. 99-107, 2013.
11. Potter, K. D., “Understanding the Origins of Defects and Variability in Composites Manufacture. In International Conference on Composite Materials (ICCM)-17, Edinburgh, UK, July 2009.
12. Sekine N., T. Takao, T. Shoji, H. Toyama, K. Kashiwazaki, N. Sugasawa, et al., “Frictional coefficients of structural materials in AC superconducting coils,” Cryogenics, Volume 41, Issue 5, pp. 379-84, 2001.
13. Syerko E, S. Comas-Cardona and C. Binetruy, “Models of mechanical properties/behavior of dry fibrous materials at various scales in bending and tension: A review,” Composites Part A: Applied Science and Manufacturing, Volume 43, Issue 8, pp. 1365-88, 2012.
14. Zhu, S. "An automated fabric layup machine for the manufacturing of fiber reinforced polymer composite,” Graduate Theses and Dissertations. Paper 13170. http://lib.dr.iastate.edu/etd/13170, 2013.